Line-resolved *M*-shell x-ray production cross sections of Pb and Bi induced by highly charged C and F ions

Y. P. Singh, D. Misra, U. Kadhane, and Lokesh C. Tribedi*
Tata Institute of Fundamental Research, Homi Bhabha Road, Colaba, Mumbai 400 005, India
(Received 6 August 2005; published 10 March 2006)

Measurement on the *M*-shell x-ray production cross sections are reported for Pb and Bi induced by the highly charged F (only on Pb) and C ions (on both). The energy of the incident ions was varied between 20 and 102 MeV. We have derived the absolute cross sections for $M\alpha\beta$ and $M\gamma$ lines as well as the total *M* x-ray cross sections. The measured cross sections are compared with available theoretical calculations, namely, the ECPSSR based on the perturbed-stationary state approximation including the effects due to the increased binding energy, Coulomb deflection (*C*), energy-loss (*E*), and relativistic (*R*) wave function. The energy shifts and the intensity ratios of $M\alpha\beta$ and $M\gamma$ lines are shown to depend on the projectile atomic number. The $M\gamma$ x-ray cross sections are unusually higher compared to the ECPSSR prediction that is primarily attributed to a dramatic enhancement in the M_3-subshell fluorescence yield owing to multiple vacancies in *N* subshells. This enhancement has been quantified and it is shown that the enhancement depends on the projectile atomic number. In addition we have derived the x-ray cross section arising due to *M*-*K*-shell electron transfer from a study of a charge state dependence of *M*-shell x-ray yields.

DOI: 10.1103/PhysRevA.73.032712 PACS number(s): 34.50.Fa

I. INTRODUCTION

The measurement of innershell ionization by charged particles has gained impetus because of the direct use of x-rays in many applied fields such as trace-element analysis, ion implantation, and fusion diagnostic studies. Inelastic collisions of charged projectiles with atoms create innershell vacancies. Among the various innershells, the *K*- and *L*-shell ionization process has been studied to a great extent. However, *M*-shell measurements are very few and most of these studies are confined to total *M*-shell cross section measurements. Only a few experiments [1–4] have been carried out which use heavy ions as projectiles and thin foil targets. Most of the earlier studies [5–7] and references in [4] were based on the low Z ion as projectiles such as *p* and He^{2+}. However, for heavy-ion experiments one has to necessarily use thin ($\sim 1-4$ $\mu g/cm^2$) targets to avoid multiple collision and electron capture contributions [8]. We have also measured the contribution in the *M*-shell x-ray yields due to *M*-shell (target) to *K*-shell (projectile) electron transfer by studying the charge state dependence of the x-ray yields. Using *H*-like and bare ions of F we found that the x-ray intensity enhances substantially over that for low charge state (filled *K*-shell for which no *M*-*K* transfer is possible in thin targets) ions (see below). The x-ray yields obtained by using these low charge state ions are essentially due to the Coulomb ionization of the *M*-shells.

The *M*-shell vacancy decays via one of the three basic processes: x-ray emission, Auger-electron emission, or Coster-Kronig transition. The rates for these processes strongly influence the final comparison of the experimental *M*-shell x-ray production cross sections with the theoretical results. Additional complications arise due to the multiple ionization in the outer shells which causes a substantial and differential change in the x-ray fluorescence yields (ω_i, for *i*th subshell) [9,10,4]. It may be noted that such enhancements, due to the interplay of the Coster-Kronig transition strength and the radiative transition probabilities, are difficult to predict by the model calculations. Therefore there is a need to measure the enhancements in the fluorescence yields, especially, in the presence of multiple outer shell vacancies. Indeed in our previous study [4] we showed a dramatic enhancement in the ω_3-value for *M*-shell ionization of Au by F ions, whereas for the other subshells such dramatic enhancements in the ω-values were not observed. Following this study, in an independent measurement Banas *et al.* [11] also showed a similar enhancement in ω_3-value of Au target. To understand this phenomenon in more details, one needs to study the systematic behavior, i.e., it is necessary to have similar studies for other projectile-target combinations as is done here for C and F ions on Pb and Bi.

We present the measurement of the total *M*-shell x-ray, $M\alpha\beta$, and $M\gamma$ cross sections for Pb in collisions with highly charged F ions as projectiles with energy ranging from 20 to 102 MeV. The existing data on total *M*-shell x-ray cross sections by Mehta *et al.* [1] for F on Pb cover a small energy range (less than 35 MeV). On the other hand, the present investigation spans a wide range of energy (20–102 MeV) and we have measured absolute cross sections for $M\alpha\beta$ as well as the $M\gamma$ lines in addition to total cross sections. To the best of our knowledge, there are only a few experiments that exist for C as projectiles. All these [2,3,12,13] measurements are confined to a low energy regime and to the measurement of total x-ray cross sections. Mitra *et al.* [13] have shown that for Au and Pb as targets, the ECPSSR [where the ECPSSR approach takes into account the energy-loss effect (*E*), as well as the Coulomb deflection (*C*), perturbed-stationary state (PSS), and relativistic (*R*) effects] [14] predictions for total x-ray cross sec-

*Email address: lokesh@tifr.res.in

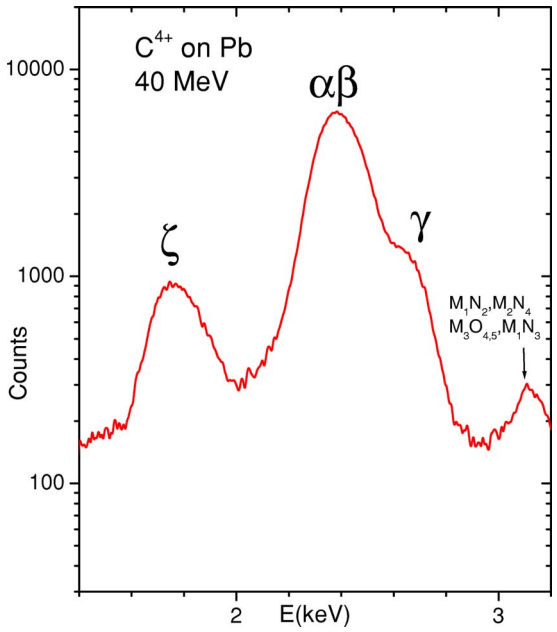

FIG. 1. (Color online) M x-ray spectrum (background subtracted) of Pb in collision with 40 MeV C^{4+}. The different components are indicated in the figure.

tions fall below the experimental cross sections by a factor as large as 4 in the studied energy range. They have attributed this discrepancy to the enhancement of the fluorescence yield as they have used an average value of the fluorescence yield. Therefore, it becomes essential to have a systematic study in a higher energy range to have a quantitative measurement on differential enhancements of the fluorescence yield for C ions as projectiles. Here we report the measurements of the total M-shell x-ray, $M\alpha\beta$, and $M\gamma$ cross sections for Pb and Bi as the targets and C ions as projectiles in the energy range of 24–72 MeV.

The collision symmetry parameter S $(=Z_p/Z_t)$ is varied between 0.109 (for F) and 0.072 (for C) signifying an asymmetric system. However, this symmetry parameter is normally defined for (target) the K-shell ionization. In the case of the M-shell (i.e, for $n=3$, n being the principal

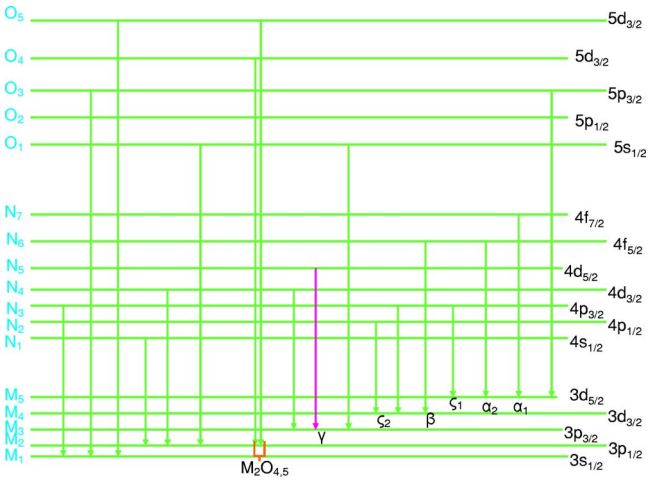

FIG. 2. (Color online) M x-ray transition lines [8,15].

TABLE I. M x-ray production cross sections ($M_{\alpha\beta}$, M_γ, and M_{total}) due to M-subshell ionization of Pb induced by F ions.

Target	Energy (MeV)	$\sigma_{\alpha\beta}$ (kb)	σ_γ (kb)	σ_{total} (kb)
Pb	20	37.3	3.7	55.2
	30	57.7	10.5	99.9
	40	84.0	12.4	138.0
	57	113.0	15.6	186.3
	76	130.0	21.3	223.1
	85	123.0	24.3	—
	95	164.0	19.9	257.6
	102	65.0	11.7	117.3

quantum number) ionization the proper parameter should be $Z_P/(Z_t/n)$, i.e., $3Z_P/Z_t$ which is, however, between 0.31 and 0.21, signifying asymmetric collision. The average values of velocity ratios v_p/v_e are between 0.43 and 0.97 for F ions and from 0.58 to 1.03 for C ions, v_p and v_e being the projectile and the M-shell electron average orbital velocity, respectively.

II. EXPERIMENTAL DETAILS AND ANALYSIS

The details of the experimental and data analysis technique are given in [4] and only the relevant discussions are included here. The experiment was performed with the 14 MV BARC-TIFR Pelletron accelerator at TIFR, Mumbai. Heavy ions of F^{4+} (20 MeV), $F^{5+,7+,8+}$ (30 MeV), $F^{6+,7+,8+,9+}$ (40 MeV), $F^{6+,8+,9+}$ (57 MeV), $F^{7+,8+,9+}$ (76 MeV), F^{7+} (85 MeV), $F^{7+,8+,9+}$ (95 MeV) $F^{8+,9+}$ (102 MeV), C^{4+} (24, 36, 40, 48), C^{5+} (60 MeV), C^{6+} (72 MeV) were used for the measurement. The mass and energy analyzed ion beams were made to fall on thin targets of Pb (1.41 $\mu g/cm^2$ for F ions and 3.8 $\mu g/cm^2$ for C ions) and Bi (1.3 $\mu g/cm^2$). These thin targets were evaporated on carbon backing-foils of thickness ~ 10 $\mu g/cm^2$.

The x-rays emitted from the target were detected by a Si(Li) detector with a 25 μm thick Be window and having 160 eV resolution at 5.9 keV. The detector was mounted inside the vacuum chamber at angles 55° to the beam direction. The thickness of the targets was obtained *in situ*, by detecting the elastically scattered particles in a surface barrier particle detector mounted at 135° and 45°.

TABLE II. M x-ray production cross sections ($M_{\alpha\beta}$, M_γ, and M_{total}) due to the M-subshell ionization of Pb induced by C ions.

Target	Energy (MeV)	$\sigma_{\alpha\beta}$ (kb)	σ_γ (kb)	σ_{total} (kb)
Pb	24	16.6	2.3	20.8
	48	56.6	5.8	68.0
	60	83.9	9.1	101.2
	72	79 700	7830	7830

TABLE III. *M* x-ray production cross sections ($M_{\alpha\beta}$, M_{γ}, and M_{total}) due to the *M*-subshell ionization of Bi induced by C ions.

Target	Energy (MeV)	$\sigma_{\alpha\beta}$ (kb)	σ_{γ} (kb)	σ_{total} (kb)
Bi	24	29	4.6	38.7
	48	52.3	4.9	61.4
	60	52.2	5.1	62.1
	72	62.7	7.4	63.9

A typical *M*-shell x-ray spectrum of Pb for 40 MeV C^{4+} ion bombardment is shown in Fig. 1. Four different groups of lines are resolvable such as $M\zeta$, $M\alpha\beta$, $M\gamma$, and $M_3O_{4,5}+M_1N_2$. The $M\alpha\beta$ line arises due to a vacancy in the M_4/M_5 subshells and $M\gamma$ is due to the filling of the M_3 vacancy (M_3N_5 transition). The *M*-shell transitions are shown in Fig. 2 [8,15]. The peak areas in the x-ray spectra were estimated using a multi-Gaussian least squares fitting program. From the measured x-ray yields the x-ray production cross sections were estimated using usual procedure [4], i.e, by dividing the target thickness, solid angles, and the intrinsic efficiency of the detector. The absolute errors in the measured cross sections were about 15–20 % arising mainly from the uncertainties in detector efficiency (~10%), solid angles (~8%), and target thickness (~8%). The background subtraction and fitting procedure introduce an additional error of about 5% or less. Errors due to counting statistics were negligible.

The equations relating x-ray production cross sections for different *M*-shell x-ray lines (σ_m^x, where *m* is any given x-ray line) to the ionization cross sections for different subshells σ_i^I ($i=1,2,3,4,5$) of the *M* shell can be found in Ref. [4]. As an example, here we write one such equation for $M\gamma$ cross section:

$$\sigma_{\gamma}^{x}=[\sigma_1^I(S_{13}+S_{12}S_{23})+\sigma_2^I S_{23}+\sigma_3^I]\omega_3\Gamma_{M_\gamma}/\Gamma_{M_3}, \qquad (1)$$

where S_{ij} are super-Coster-Kronig factors calculated by McGuire [16] and Γ_{M_i} are radiation widths for i_{th} subshell calculated by Bhalla [17].

These above equations have been used to calculate theoretical x-ray cross sections for different lines. The required subshell resolved ionization cross sections were taken from ECPSSR calculations to derive x-ray cross sections which are then plotted against the experimental x-ray cross sections. The measured x-ray cross sections are tabulated in Tables I–III.

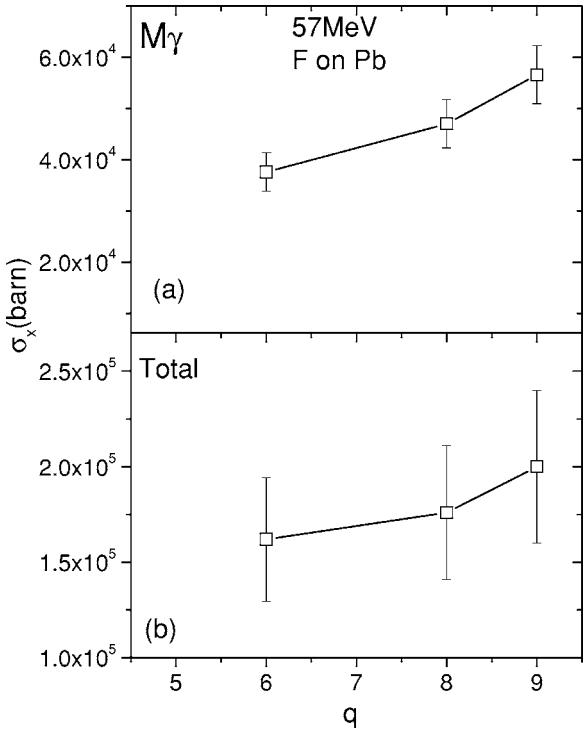

FIG. 3. Projectile charge state dependence of *M* x-ray cross sections for 57 MeV F on Pb: (a) $M\gamma$ line; (b) total x rays.

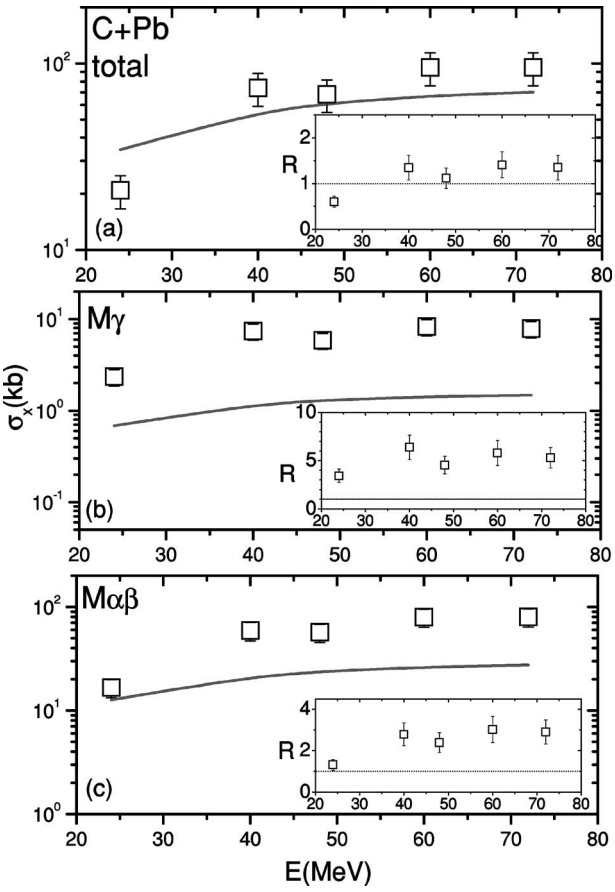

FIG. 4. X-ray production cross sections: (a) total, (b) $M\gamma$ line, and (c) $M\alpha\beta$ lines for C on Pb. The solid lines correspond to the ECPSSR predictions. The insets show the ratio of the data to the calculations.

III. RESULTS AND DISCUSSIONS

First we show the results (Fig. 3) obtained in the measurements of the *M*-shell x-ray cross sections as a function of projectile charge state (q) dependence. Enhancement in the cross sections has been observed for *H*-like F ($q=8$) or bare F ions ($q=9$) compared to cross sections obtained for ions

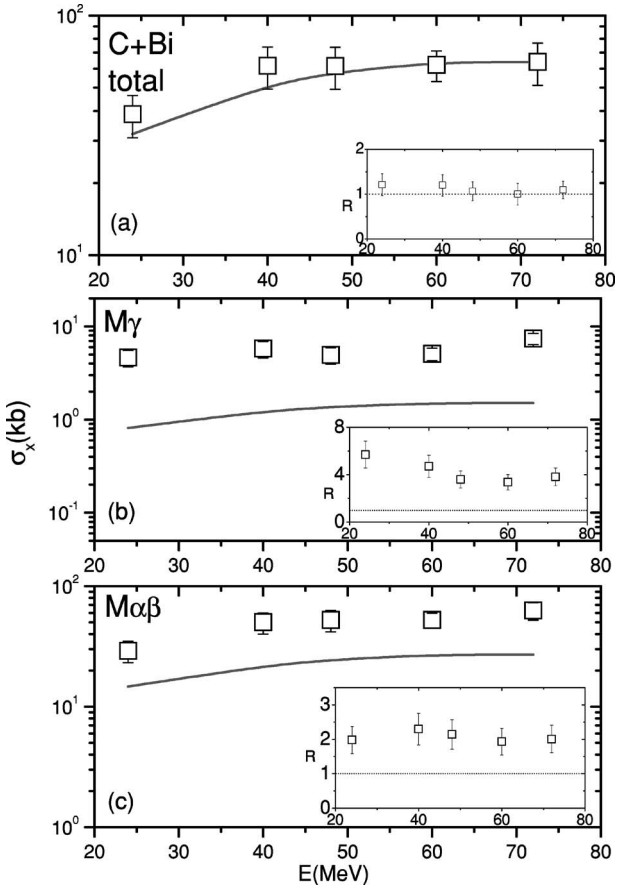

FIG. 5. Same as above in Fig. 3 except for Bi as the target.

with their K-shell completely filled (i.e., $q \leqslant 7$). This is due to the transfer of the M-shell target electron to the K shell of the ion and known as the M-K electron transfer. A typical example is shown in Fig. 3 for 57 MeV F ions on Pb. For the F ions the contribution in the $M\gamma$ yields due to the M-K transfer is found to be about 25% of M ionization (see Fig. 3). The transfer cross section depends on the projectile atomic number, and the binding energy of initial (M) and final (K of projectile) states. Therefore it can be estimated that M-K transfer would be much less for C ions. The rest of the paper deals with the x-ray cross sections due to only ionization (i.e., completely filled K-shell ions).

The $M\alpha\beta$, $M\gamma$, and total M-shell x-ray production cross sections are plotted in Figs. 4–6 as a function of the beam energy for C on Pb (Fig. 4) and Bi (Fig. 5) and F on Pb (Fig. 6). The ECPSSR calculations [14] are shown by solid continuous lines. The insets in the figures show the ratio (R) of the experimental data to the ECPSSR predictions. For C ions, the ECPSSR closely agrees with the total x-ray cross sections for Pb [see Fig. 4(a)] and is in a very good agreement with the total x-ray cross sections for Bi [see Fig. 5(a)]. The ratio R is approximately 1.0 throughout the energy range. This is in sharp contrast to the results obtained by Mitra *et al.* [13] for C on Pb for total x-ray cross sections in a slightly lower energy range. They found that the measured cross sections are higher than the ECPSSR predicted cross sections by a factor of 4.0. The use of thick target could be a possible reason for such apparent deviation in Ref. [13].

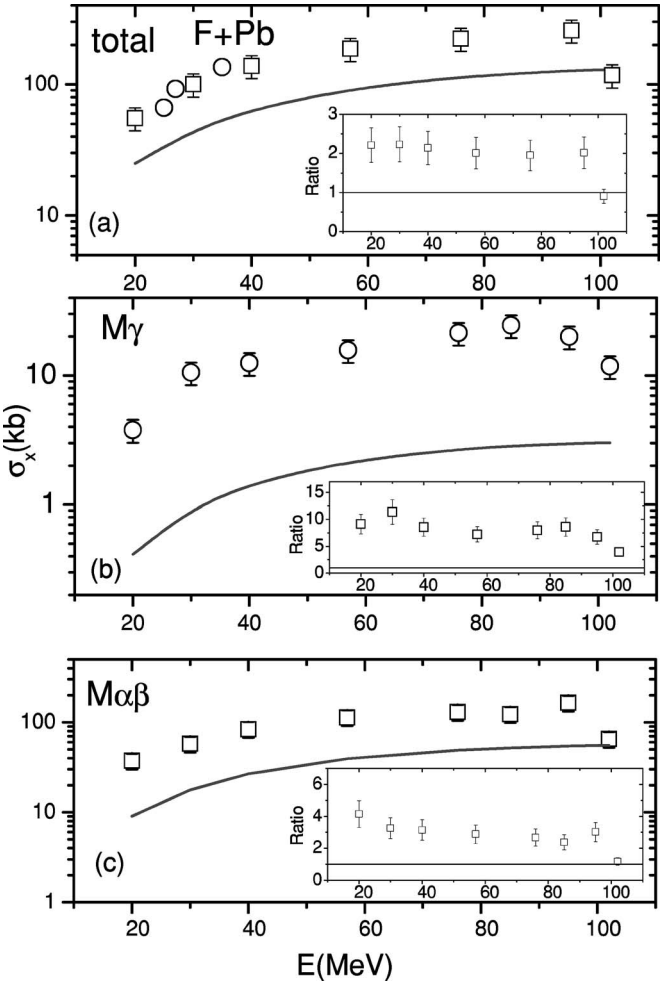

FIG. 6. X-ray production cross sections of (a) total, (b) $M\gamma$, and (c) $M\alpha\beta$ induced by F as projectile. The solid lines correspond to the ECPSSR predictions. The open circles in (a) are from Ref. [1]. The insets show the ratio of the data to the calculations.

However, our data show overall reasonable agreement with the ECPSSR predictions. The total cross sections for F on Pb are shown in Fig. 6(a) together with the only existing total cross section data for low energy F ions [1] [see open circles in Figs. 6(a)] are also plotted. It can be seen that the present experimental cross sections are in fairly good agreement with the earlier data sets. However, the calculated total cross sections fall below the experimental data by about a factor of 2 except at the highest energy. The deviation of the experimental cross sections from the calculated cross sections is more for F ions. This can be seen from the dotted line drawn through the ratio data plotted in the inset. For $M\alpha\beta$, this deviation is by an approximate factor of 3 for F on Pb [see Fig. 6(c)], 2.5 for C on Pb [see Fig. 4(c)], and 2 for C on Bi [see Fig. 5(c)]. However, multiple ionization in outer shells causes the enhancement in the fluorescence yields for inner shells, and can be, in principle, estimated based on Larkins' statistical principle [18] which have been applied in numerous studies for K- and L-shell ionizations. The information on the vacancy configuration in the outer shells, i.e., N- and O-shells simultaneous with the M-shell vacancy is necessary to estimate the enhancement in the subshell fluorescence

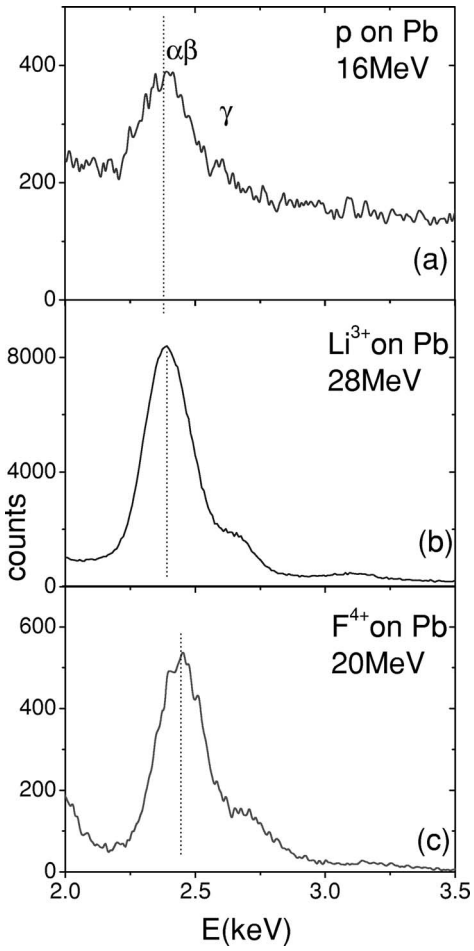

FIG. 7. The *M*-shell x-ray spectra, showing the $M\alpha\beta$ line of Pb for different projectiles: (a) 16 MeV proton, (b) 28 MeV Li^{3+}, and (c) 20 MeV F^{4+} are shown. The vertical line marks the peak energy of the $M\alpha\beta$ line.

yields. Although the energy shifts and the intensity ratios are measured (see below), the exact determination of the vacancy configuration in outer shells is complicated since too many subshells are involved. However, one expects some enhancements in the ω_4 values which could be typically about 10–30 % based on the previous studies of *K*- [19,20] and *L*-shell [21] measurements. This explains only a part of the deviation from theory which is about a factor of 2 or 3 higher than the experimental data for $M\alpha\beta$ [Figs. 4(c), 5(c), and 6(c)]. Most of the deviation with the $M\alpha\beta$ data, therefore, indicate the limitation of the ECPSSR model to predict *M*-subshell ionization cross sections.

$M\gamma$ cross section. The most striking feature of these figures is a very large deviation of $M\gamma$ cross sections from the calculated cross sections [see Figs. 4(b), 5(b), and 6(b)]. In each case the measured data fall well above the model prediction. These deviation factors are approximately 8, 5, and 4 for F on Pb [see Fig. 6(b)], C on Pb [see Fig. 4(b)], and C on Bi [see Fig. 5(b)] respectively. This will be discussed later in detail.

In Figs. 7(a)–7(c) we display the *M*-shell x-ray spectra for Pb obtained by different projectiles such as *p*, Li, and F ions. The shift of the $M\alpha\beta$ and $M\gamma$ lines are clearly visible compared to that for protons, as indicated by vertical lines which correspond to the $M\alpha\beta$ peak for proton impact. These shifts for $M\alpha\beta$ lines are explicitly plotted in Fig. 8 as a function of projectile Z_p. These are found to increase very rapidly with Z_p. In the case of F, this shift is about 50 ± 10 eV for $M\alpha\beta$ lines ($\Delta E_{\alpha\beta}$) and about the same for the $M\gamma$ line. The shifts for Li and C ions are found to be about 10 and 30 eV, respectively, for $M\alpha\beta$ lines. These energy shifts are due to the existence of the multiple vacancies in the outer shells at the time of x-ray emission.

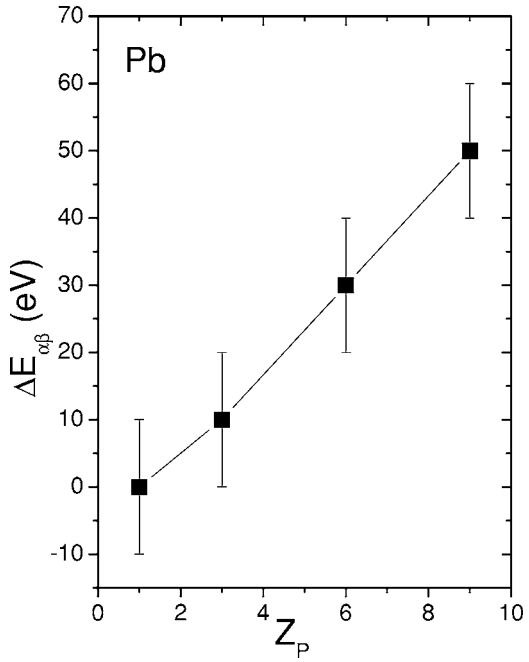

FIG. 8. The energy shifts of the $M\alpha\beta$ line as a function of Z_P.

To understand the abnormal behavior shown by $M\gamma$ cross sections, in Fig. 9, we show the intensity ratios $I(\gamma)/I(\alpha\beta)$ for F on Pb, C on Pb, and C on Bi. For F ions this ratio varies from 0.21 to 0.35 [see Fig. 9(a)]. For comparison the ECPSSR calculations are also plotted as solid lines. It can be observed that the data are always higher than the calculations. In fact the discrepancy between the data and calculations is much more for F ions than that for C ions for the similar incident energies. The ratio of experimental data to the calculation is about 7 for F ions, while it is only about 2 for C ions. Therefore it strongly depends on Z_P. However, the deviation is caused partly due to multiple vacancies in outer shells and partly due to the inability of the theory to reproduce the M_3 and $M_{4,5}$ vacancy probability.

The energy shifts together with higher $I(\gamma)/I(\alpha\beta)$ intensity ratios indicates the multiple ionization in the outer shells together with *M*-shell vacancies in the target. This, in turn, results in the enhancement of the fluorescence yields. In particular, it is evident from the present data that the cross section for $M\gamma$ (i.e., M_3-N_5), which arises from the M_3 vacancy, is largely influenced by the multiple vacancy in outer shells and therefore the fluorescence yield for the M_3 subshell is enhanced dramatically. What happens is that due to the multiple ionization in the outer shells like *N* and *M*, some

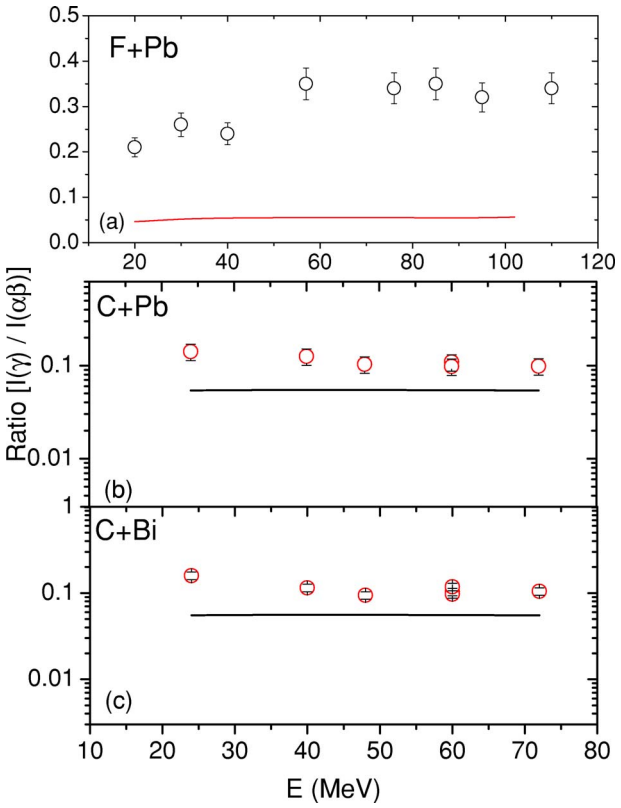

FIG. 9. (Color online) The intensity ratios $[I(\gamma)/I(\alpha\beta)]$ of $M\gamma$ to $M\alpha\beta$ lines for (a) F on Pb; (b) C on Pb; (c) C on Bi shown as a function of different incident energies of ions. The ECPSSR prediction is shown as a line.

of the Coster-Kronig (CK) transitions are less probable and therefore the radiative process dominates giving rise to higher x-ray cross sections compared to the model predicted cross sections. In Table IV, we show some of the values of CK transition probabilities [16] and the subshell fluorescence yields for Pb and Bi. It is worth noting here that the CK transition probability S_{35} (this arises due to a vacancy in M_3 subshell), is much higher (almost a factor of 150 large for Pb and almost a factor of 140 large for Bi) compared to ω_3. Therefore any multiple ionization in the N subshells (especially in N_6 and N_7) will reduce the S_{35} CK channel drastically as a result of the blocking of the particular $M_3-M_5N_{6,7}$ channel, giving rise to a larger ω_3 value. However, in the case of the vacancy in the M_4, the relevant parameter, i.e., ω_4 and the corresponding CK rate S_{45}, have comparable values and therefore there is no drastic enhancement in the ω_4. So no such dramatic deviations are observed for the $M\alpha\beta$ cross sections.

TABLE IV. Atomic parameters related to M_3 and M_4 vacancy filling used in the calculation, i.e., the CK rates and fluorescence yields (Ref. [16]).

Element	ω_3	$S_{M3,4}$	$S_{M3,5}$	ω_4	$S_{M4,5}$	ω_5
Pb	0.005048	0.099	0.758	0.0314	0.0378	0.0308
Bi	0.00533	0.094	0.750	0.033	0.035	0.0325

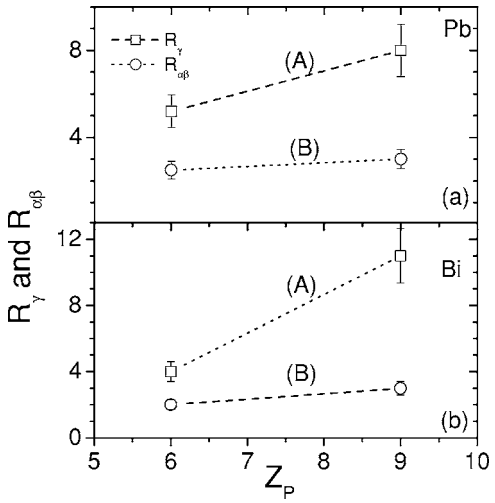

FIG. 10. The ratios (R_γ and $R_{\alpha\beta}$) of the experimental data to the ECPSSR predictions for $M\gamma$ as well as $M\alpha\beta$ x-ray cross sections as a function of Z_P: (a) Pb and (b) Bi. Lines (denoted as A and B) are to guide the eyes.

Therefore, for the $M\gamma$ line, the average (over energy) enhancement factors (*w.r.t.* the ECPSSR predictions) (R_γ, see Fig. 10) for C on Pb and Bi are 5.2 and 4.2, respectively. But it is shown above that the ECPSSR itself underestimates the $M\alpha\beta$ cross section by a factor ($R_{\alpha\beta}$, see Fig. 10) of 2.5 (C on Pb) or 2.0 (C on Bi) and one can assume that this could be taken as a practical measure of the deviation of the theory even for the $M\gamma$ cross sections. Therefore, the rest of the

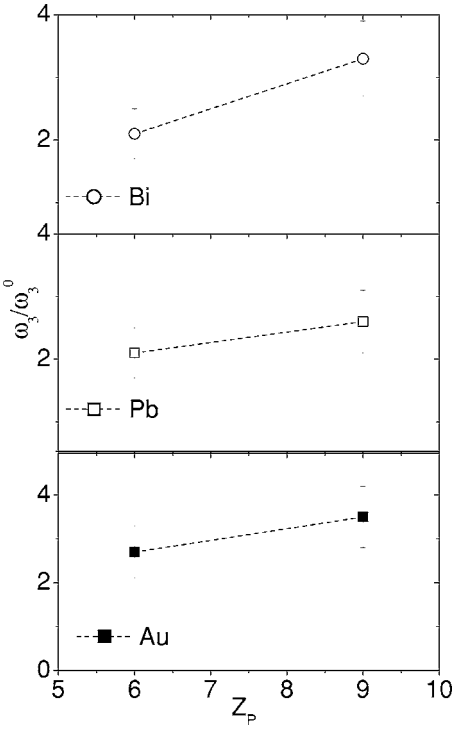

FIG. 11. The derived average enhancement in the fluorescence yield for the M_3 subshell, i.e., ω_3/ω_3^0: obtained by dividing the ratios in Fig. 9, i.e., R_γ by $R_{\alpha\beta}$. The average values for Au are taken from our previous work [4].

deviation $R_\gamma/R_{\alpha\beta}$ can be taken as a measure of (ω_3/ω_3^0), i.e., the average enhancement in the fluorescence yield with respect to the single hole value (ω_3^0). For example, it was found to be 4.2/2.0 2.1 for C on Bi. The exactly same enhancement was seen also for C+Pb. Similarly, for F on Pb the ECPSSR prediction is about a factor of 8.0 (R_γ) lower compared to the $M\gamma$ cross sections and a factor of 3.5 $(R_\alpha\beta)$ lower compared to $M\alpha\beta$ data. Therefore the estimated enhancement, ω_3/ω_3^0, is about 2.6. From our earlier measurements [22] of the $M\alpha\beta$ and $M\gamma$ x-ray cross sections for F on Bi we estimated that the average enhancement factors are: 11 for R_γ, 3.0 for $R_\alpha\beta$ giving in ω_3/ω_3^0 is about 3.6 (see Fig. 11). Therefore it can be seen that the dramatic enhancement in the fluorescence yield of the $M\gamma$ line depends on the projectile atomic number Z_P. The ω_3/ω_3^0 values for all three targets, i.e., Bi, Pb, and Au (taken from [4]) studied are plotted as a function of Z_P, in Figs. 11(a)–11(c). It is found that ω_3/ω_3^0 increases with Z_P and all three targets, with quite similar slopes.

Independently, Banas *et al.* [11] have also found the net enhancement in the fluorescence yield of M_3 due to the closing of the CK transition of $M_3-M_5N_{6,7}$. They argue that the change of electron binding energies in the multiple ionized atoms, that causes the observed x-ray shifts, can have a strong effect on the CK transitions, in particular, for those transitions for which the CK electrons have rather low energies, being of the order of energy shifts of the electron binding energies. An important effect, which can occur in multiply ionized atoms, is simply a closing of the CK transition when the energy of CK electrons becomes negative. Such CK transitions are thus energetically forbidden and do not contribute to the total CK yields. Consequently, the total decay widths are modified, which influences in turn both x-ray fluorescence and CK yields. Our measurement is in qualitative agreement with this study [11].

IV. CONCLUSIONS

M-shell x-ray production cross sections (due to ionization) for Pb and Bi induced by the highly charged F ions (only Pb) and C ions have been measured. F and C ions have the energy range 20–102 MeV and from 24–72 MeV, respectively. The cross section for $M\alpha\beta$ and $M\gamma$ lines together with total *M*-shell x-ray cross sections are reported. The measured energy shifts of the x-ray lines and the enhanced intensity ratios, $I(\gamma)/I(\alpha\beta)$, compared to the single hole value indicate substantial multiple vacancies in the outer subshells such as *N* subshells. X-ray production cross sections for the $M\gamma$ line were observed to be substantially higher than the cross sections predicted by the ECPSSR. By comparing this dramatic enhacement in the cross sections with the corresponding deviations for the $M\alpha\beta$ data we have derived the enhancement factor in the M_3-subshell fluorescence yield owing to multiple vacancies in *N* subshells. The dramatic enhancement in the ω_3-value has been quantified. It has been found that for all the targets studied this enhancement strongly depends on the projectile atomic number. A complete summary has been presented for all three target elements: Au, Pb, and Bi, using some of our previously published data.

ACKNOWLEDGMENTS

We would like to thank K. V. Thulasiram and D. Mitra for their help during the experiment and the machine staff for smooth running of the accelerator.

[1] R. Mehta, J. L. Duggan, F. D. McDaniel, M. C. Andrews, G. Lapicki, P. D. Miller, L. A. Rayburn, and A. R. Zander, Phys. Rev. A **28**, 2722 (1983).
[2] Y. C. Yu, H. L. Sun, J. L. Duggan, F. D. McDaniel, J. Y. Jin, and G. Lapicki, Phys. Rev. A **52**, 3836 (1995).
[3] M. C. Andrews, F. D. McDaniel, J. L. Duggan, P. D. Miller, P. L. Pepmiller, H. F. Krause, T. M. Rosseel, L. A. Rayburn, R. Mehta, and G. Lapicki, Phys. Rev. A **36**, 3699 (1987).
[4] Yeshpal Singh and Lokesh C. Tribedi, Phys. Rev. A **66**, 062709 (2002).
[5] Ch. Herren, B. Boschung, J.-Cl. Dousse, B. Galley, J. Hoszowska, J. Kern, Ch. Rheme, M. Polasik, T. Ludziejewski, P. Rymuza, and Z. Sujkowski, Phys. Rev. A **57**, 235 (1998).
[6] J. L. Price, J. L. Duggan, F. D. McDaniel, G. Lapicki, and R. Mehta, Phys. Rev. A **37**, 365 (1988).
[7] M. Sarkar, H. Mommsen, W. Sarter, and P. Schurkes, J. Phys. B **14**, 3163 (1981).
[8] T. J. Gray in *Methods of Experimental Physics*, edited by P Richard (Academic, New York, 1980), Vol. 17, p. 193.
[9] W. Jitschin, R. Hippler, K. Finck, R. Schuch, and H. O. Lutz, J. Phys. B **16**, 4405 (1983), and references therein.
[10] Y. P. Singh, D. Mitra, Lokesh C. Tribedi, and P. N. Tandon, Phys. Rev. A **63**, 012713 (2001).
[11] D. Banas, J. Braziewicz, M. Czarnota, I. Fijal, M. Jaskola, A. Korman, W. Kretschmer, M. Pajek, and J. Semaniak, Nucl. Instrum. Methods Phys. Res. B **205**, 139 (2003).
[12] T. Czyzewski, L. Glowacka, M. Jaskola, J. Brazewicz, M. Pajek, J. Semaniak, M. Haller, R. Karschnik, W. Kretschmer, A. P. Kobzev, and D. Trautmann, Nucl. Instrum. Methods Phys. Res. B **52**, 109 (1996).
[13] D. Mitra, A. C. Mandal, M. Sarkar, D. Bhattacharya, P. Sen, and G. Lapicki, Nucl. Instrum. Methods Phys. Res. B **183**, 171 (2001).
[14] W. Brandt and G. Lapicki, Phys. Rev. A **23**, 1717 (1981).
[15] J. A. Bearden Rev. Mod. Phys. **39**, 78 (1967).
[16] E. J. McGuire, Phys. Rev. A **5** 1043 (1972).
[17] C. P. Bhalla J. Phys. B **3**, 916 (1970).
[18] F. P. Larkins, J. Phys. B **4**, L29 (1971).
[19] J. Hall, P. Richard, P. L. Pepmiller, D. C. Gregory, P. D. Miller, G. D. Moak, C. M. Jones, G. D. Alton, L. B. Bridwell, and C. J. Sofield, Phys. Rev. A **33**, 914 (1986).
[20] L. C. Tribedi, K. G. Prasad, P. N. Tandon, Z. Chen, and C. D. Lin, Phys. Rev. A **49**, 1015 (1994).
[21] B. B. Dhal, A. K. Saha, Lokesh C. Tribedi, K. G. Prasad, and P. N. Tandon, J. Phys. B **31**, L807 (1998).
[22] Yeshpal Singh and Lokesh C. Tribedi, Nucl. Instrum. Methods Phys. Res. B **205**, 794 (2003).